JOURNAL OF SOLID STATE CHEMISTRY 15, 68–78 (1975)

A Microdomain Description of Defective Fluorite-Type Phases $Ca_xM_{1-x}O_{2-x}$(M = Zr, Hf; x = 0.1–0.2)

J. G. ALLPRESS AND H. J. ROSSELL

CSIRO Division of Tribophysics, University of Melbourne, Parkville, Victoria, 3052, Australia

Received October 30, 1974

Electron diffraction patterns from cubic solid solutions of lime in zirconia and hafnia contain weak diffuse features in addition to the strong reflections expected from the fluorite structure type. A comparison of these features with those found in patterns from annealed specimens suggests that the solid solutions contain domains embedded coherently in a number of specific orientations within the cubic matrix. Each domain is about 30 Å in diameter, and its structure corresponds to that of $CaHf_4O_9$. Calculations based on this model agree with the observed diffraction data.

1. Introduction

The fluorite-type solid solutions obtained by reacting zirconia or hafnia with a variety of oxides such as lime and yttria are stable over extended ranges of composition and temperature and are of considerable importance in ceramic and solid state electrolyte technology. These materials are generally referred to as *stabilized zirconias* (*or hafnias*). In the case of lime stabilization, their compositions can be expressed by the formula $Ca_xM_{1-x}O_{2-x}$, where M = Zr or Hf and x lies in the range 0.1–0.2.

These cubic solid solutions are oxygen-deficient with respect to the fluorite composition MO_2, and it is generally agreed that this discrepancy is accommodated by the presence of vacant sites in the oxygen sublattice (*1*, *2*). The degree to which these vacancies are regularly arranged very much depends on the temperature and thermal history of the specimen. There is no evidence for long-range order in $Ca_xM_{1-x}O_{2-x}$ at temperatures above about 1650 and 1750°K for M = Zr and Hf, respectively (*3*, *4*). Ordering in the CaO–HfO_2 system is relatively rapid at temperatures below about 1700°K, and there are at least three ordered phases, referred to as ϕ, ϕ_1, and ϕ_2 (*4–6*), in which $x = 0.2222$, 0.2000, and 0.2400, respectively (*7–9*). Ordering in the lime–zirconia system appears to occur at rather lower temperatures, and is correspondingly slower. However, phases analogous to ϕ_1 and ϕ_2 have been reported (*3*, *10*).

X ray powder diffraction patterns from the high-temperature disordered phases contain only the reflections due to Bragg scattering from the fluorite-type lattice. However, additional diffuse features have been observed in single-crystal X ray and electron diffraction patterns (*10*, *11*) and also in powder neutron diffraction data (*11*, *12*). These data have been interpreted in terms of the relaxation of oxygen atoms away from their ideal fluorite positions and the formation of ordered zones or domains.

This paper presents some further observations of the diffraction of electrons from solid solutions of lime in zirconia and hafnia, including data from partially and completely ordered samples of ϕ_1, $CaHf_4O_9$. The results support the domain concept proposed by Carter and Roth (*11*); moreover, they indicate that the ordering within the domains corresponds to that which exists in ϕ_1.

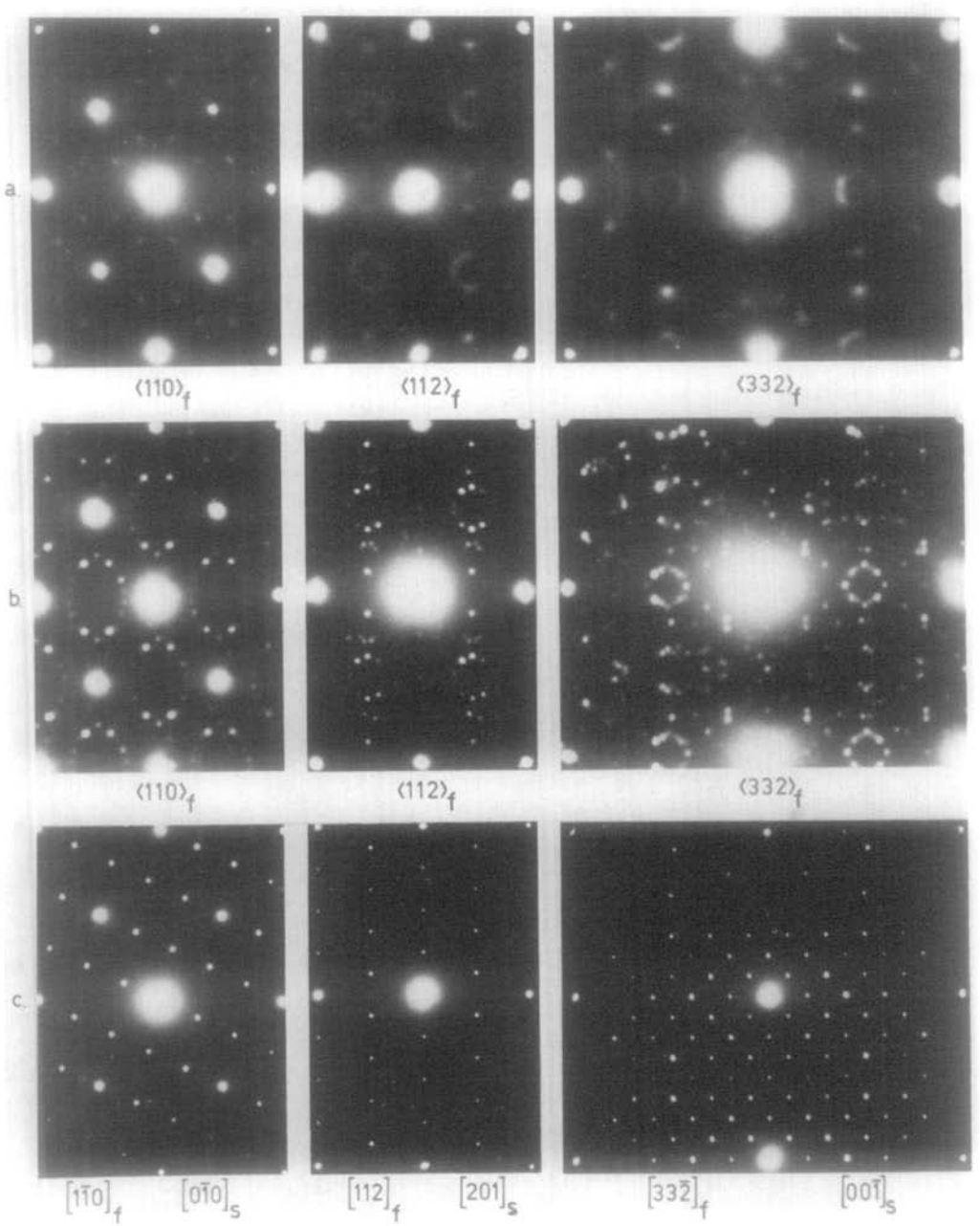

FIG. 1. Electron diffraction patterns from $Ca_xM_{1-x}O_{2-x}$, showing various stages in the ordering process. The fluorite indices of the zone axes of the patterns are given with subscript *f*. (a) Diffuse scattering from disordered phases with $M = Zr$; $\langle 110\rangle_f$, $x = 0.2$; arc-melted sample, annealed at 1250°K for 170 hr. $\langle 112\rangle_f$, $x = 0.2$; solar-melted sample, no annealing, $\langle 332\rangle_f$, $x = 0.15$; sample sintered at 1900°K, furnace cooled. (b) Sharp superlattice spots from partially ordered multidomain structures with $M = Hf$, $x = 0.2$; the samples were arc-melted and annealed at 1600°K for 3 hr. (c) Single crystal patterns from ϕ_1, $CaHf_4O_9$, prepared by arc-melting and annealing at 1670°K for up to 92 hr; the monoclinic indices of the zone axes of these patterns are given with subscript *s*.

2. Experimental

Most of the samples were prepared from Ugine Kuhlmann zirconia (hafnia-free grade) and hafnia (containing 8 moles% ZrO_2) and calcium carbonate of analytical reagent quality. Weighed amounts of the starting materials were thoroughly mixed and finely ground, pressed into small pellets, and fired at 1250°K for several hours (to decompose the carbonate) before further treatment. The samples were subsequently sintered at above 1800°K or melted in an arc or solar furnace, and annealed at various temperatures below 1700°K.

Thin fragments were prepared by crushing the products, and these were examined in a JEM 200A electron microscope equipped with a goniometer stage and operated at 200 kV.

3. Observations

Some electron diffraction patterns from lime–zirconia solid solutions are shown in Fig. 1a. In addition to a set of strong reflections (circular white patches) characteristic of the fluorite-type subcell, there are a number of weaker spots and circular features whose positions are not simply related to those of the subcell spots. The arrangement of these *diffuse* maxima was relatively insensitive to variations in lime content in the range $x = 0.1$–0.2, and was unaffected by the method of preparation (arc-melting, solar-melting, or sintering of the component oxides). The effect of annealing the samples for short periods at low temperatures (e.g., 1 week at 1270°K) was merely to sharpen the diffuse maxima to some extent.

Electron micrographs from lime–zirconia solid solutions, recorded under approximately two-beam diffracting conditions, contained contrast that was mottled on a scale of about 50 Å (Fig. 2a).

Disordered lime–hafnia samples (i.e., those not annealed in the temperature range 1500–

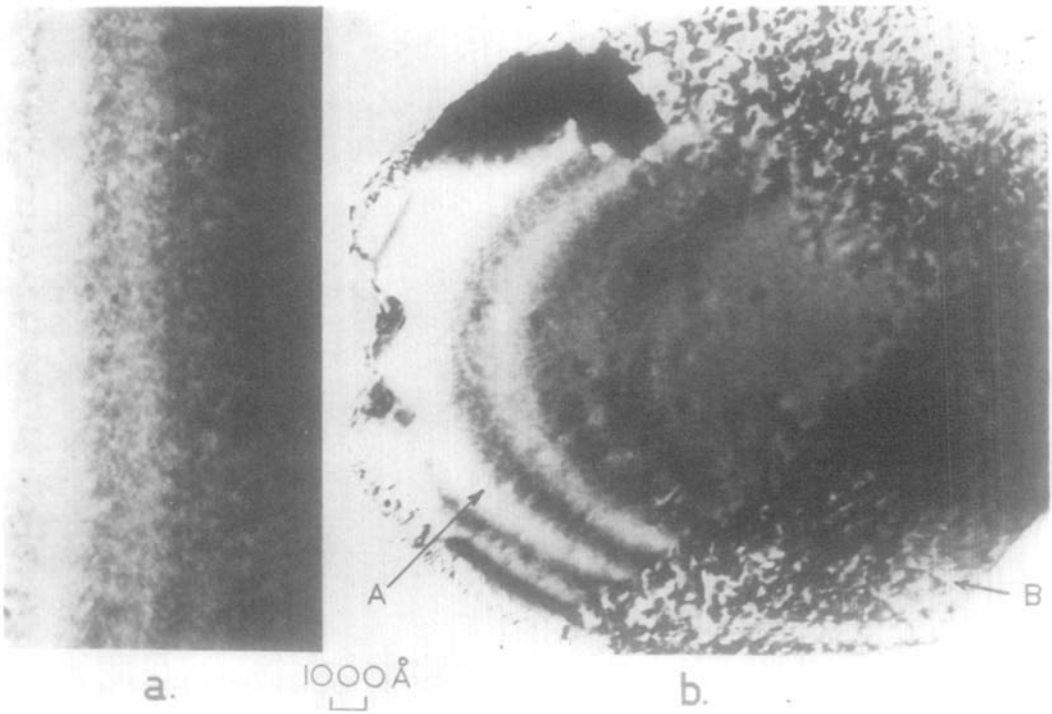

FIG. 2. Electron micrographs from $Ca_xM_{1-x}O_{2-x}$, recorded using two-beam conditions and a diffracting vector of the type 220_f. (a) $M = Zr$, $x = 0.2$; arc-melted sample, annealed at 1250°K for 170 hr; the $\langle 110 \rangle_f$ diffraction pattern was recorded from the same crystal. (b) $M = Hf$, $x = 0.2$; arc-melted sample, annealed at 1500°K for 16 hr; region A is disordered as in (a), region B contains larger domains, and the contrast is mottled on a scale of about 300 Å.

1700°K) gave patterns very similar to those in Fig. 1a; some examples are shown in Fig. 5b (the 000 spot lies in the center of the patterns in Fig. 1, and at the bottom left corner of those in Figs. 4 and 5). However, when samples containing 20 mole% lime ($x = 0.2$) were annealed at 1500–1700°K for short periods (e.g., 3 hr at 1600°K), the diffuse scattering in diffraction patterns was replaced by complex arrays of sharp spots (Fig. 1b). Many of these spots lay in positions that were occupied by diffuse maxima in patterns from the disordered samples (Fig. 1a). At the same time, the contrast in electron micrographs of thin fragments altered considerably. Fig. 2b shows a micrograph of a partly transformed crystal containing a region *A* in which the contrast is similar to that in Fig. 2a, and a region *B* where the contrast is mottled on a much coarser scale. Diffraction patterns from regions *A* and *B* were similar to those shown in Figs. 1a and 1b, respectively.

After longer periods of annealing in the same temperature range (e.g., 92 hr at 1670°K), many fragments were transformed entirely to an ordered structure and gave diffraction patterns typical of single crystals of the monoclinic phase ϕ_1, $CaHf_4O_9$ (*7*). Some of these patterns are shown in Fig. 1c; some of the reflections coincide with spots that occur in the corresponding patterns in Fig. 1b.

A similar sequence of patterns was obtained from ZrO_2–20 mole% CaO samples after very long periods of annealing at 1300–1400°K. For example, patterns similar to those in Figs. 1b and 1c were obtained after annealing for 1000 and 3600 hr, respectively. These patterns confirmed that the reciprocal lattice of the ordered phase $CaZr_4O_9$ was the same as that of ϕ_1.

4. Interpretation

The diffuse intensity in the electron diffraction patterns shown in Fig. 1a is similar in many respects to that observed in data from transition metal carbides and nitrides (*13*), for which an interpretation based on short-range order has been given (*14*). However, approximate measurement of the half-widths of the diffuse maxima indicates that in the present case at least, the scattering must come from ordered regions about 30–50 Å in diameter. While it is, in principle, possible to extend the short-range order description (by increasing the number of parameters) to cope with correlations over distances of tens of atomic diameters, we have chosen in the first instance to explore the validity of an alternative microdomain description. There is a fundamental difference between these two approaches, in that the first sets out to describe (in statistical terms) an atomic environment that is the same at all lattice points, while the second treats the structure as an agglomeration of discrete regions of complete order. The microdomain description is essentially heterogeneous, and appears to be applicable to the present data because:

(a) The geometry of the diffuse scattering is not sensitive to composition in the range of interest. This is expected if the effect of reducing lime content is to increase the distance between domains rather than to alter their structure.

(b) Electron micrographs (Fig. 2) contain mottled contrast, consistent with a heterogeneous microstructure.

For the lime–hafnia samples, annealing results in a separation of the diffuse maxima in the electron diffraction patterns (similar to Fig. 1a) into closely spaced sharp spots (Fig. 1b), accompanied by an increase from ~50Å to ~300 Å in the scale of the mottled contrast in electron micrographs (Fig. 2b). These observations are consistent with a model involving the growth of domains of ordered structure within the fluorite-type matrix. The final stage of this growth process is the formation of single crystal fragments of the fluorite-related structure ϕ_1 (Fig. 1c). Therefore, it is probable that the structures of the disordered and partly transformed samples are related to that of ϕ_1, and we have investigated a model in which domains of ϕ_1 exist in a variety of orientations in a fluorite-type matrix.

4.1. The Geometry of the Diffraction Patterns

The phase ϕ_1 is monoclinic, space group $C2/c$, with $a = 17.698$ Å, $b = 14.500$ Å,

$c = 12.021$ Å, $\beta = 119.47°$ (*7*). The axes of its unit cell are related to those of the fluorite subcell by the expression

$$\begin{pmatrix} a \\ b \\ c \end{pmatrix}_{\phi_1} = \begin{pmatrix} 2 & 2 & 2 \\ -2 & 2 & 0 \\ -\frac{3}{2} & -\frac{3}{2} & 1 \end{pmatrix} \begin{pmatrix} a_1 \\ a_2 \\ a_3 \end{pmatrix}_f. \quad (1)$$

In the case of an arc-melted sample of HfO_2–20 mole% CaO, the cubic parameter, derived from powder X ray data, was $a_f = 5.117 \pm 0.001$ Å, and the corresponding parameters for an undistorted monoclinic cell of ϕ_1 are $a = 17.726$ Å, $b = 14.473$ Å, $c = 12.000$ Å, $\beta = 119.50°$. This indicates that the distortion introduced by ordering cations and vacancies on the superlattice of ϕ_1 is quite small and it would be expected that domains of the ordered phase could exist in a fluorite-type matrix without inducing large strains, at least for small domain sizes.

Equation (1) indicates that the unique b-axis of the supercell lies parallel to the $[\bar{1}10]_f$ direction of the subcell and it can be shown that this direction uniquely defines the supercell orientation. Nucleation of isolated crystallites of ϕ_1 within the fluorite matrix would involve orientation of the unique axis parallel to any one of the 12 $\langle 110 \rangle_f$ directions with (supposedly) equal probability. If this is the case, the electron diffraction pattern from a fragment (which is a

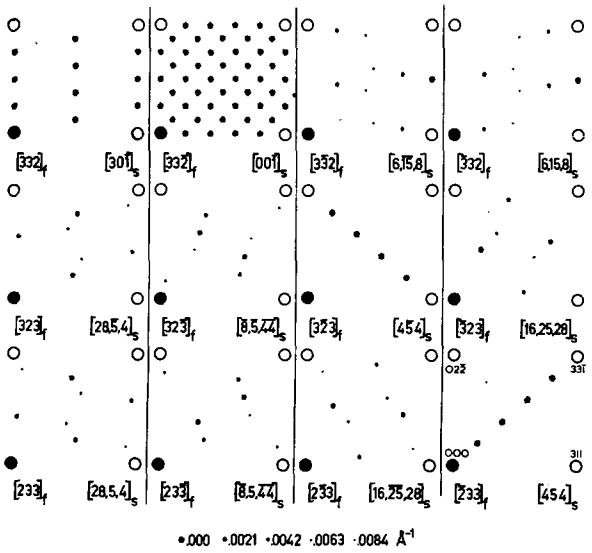

FIG. 3. Positions of Bragg reflections from ϕ_1 that lie within 0.01 Å^{-1} of the 12 $\langle 332 \rangle_f$ reciprocal lattice planes. The large circles represent subcell reflections, the filled circle being the 000 beam in each case. Fluorite indices of these reflections are given in the pattern on the lower right. The supercell reflections are denoted by smaller circles whose size indicates their distance from the subcell plane, as shown by the key below the figure. Both fluorite (subscript f) and supercell (subscript s) indices are given for each reciprocal lattice plane.

FIG. 4. Computed and experimental multidomain electron diffraction patterns from ϕ_1. (a) Expected positions of Bragg reflections that lie within 0.01 Å^{-1} of the $\langle 110 \rangle_f$, $\langle 112 \rangle_f$, and $\langle 332 \rangle_f$ subcell planes; each pattern is the superposition of 12 patterns of the kind shown in Fig. 3; the large circles represent subcell reflections, smaller circles are supercell reflections, their size indicating distance from the subcell plane, as in Figure 3; fluorite indices of some of the subcell reflections are given. (b) Kinematic intensities of the reflections plotted in (a); the area of the circles representing supercell spots is proportional to calculated intensity; reflections whose calculated intensity was less than about 2% of the maximum supercell intensity are omitted. (c) The data in (b), plotted after including the effects of double diffraction from the subcell reflections. (d) Experimental data from fragments of HfO_2–20 mole% CaO, arc-melted and annealed for 3 hr at 1600°K.

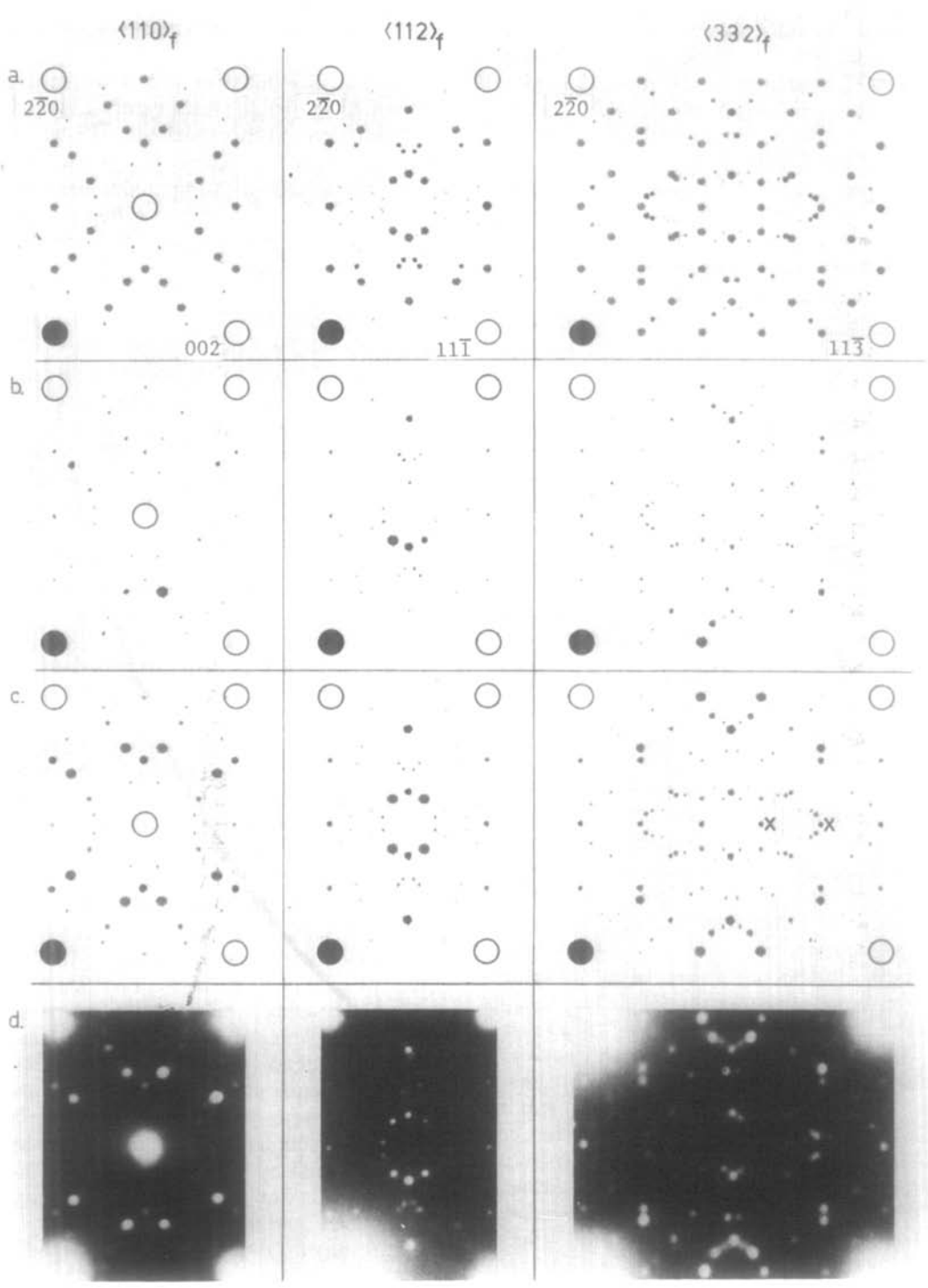
⟨110⟩f
⟨112⟩f
⟨332⟩f
a.
b.
c.
d.
2$\bar{2}$0
2$\bar{2}$0
2$\bar{2}$0
002
11$\bar{1}$
11$\bar{3}$
X
X

Fig. 4

single crystal with respect to the fluorite-type subcell) should contain contributions from domains of ϕ_1 that occur in 12 precisely known orientations in about equal numbers. Therefore, the observed pattern should be a superposition of patterns from domains in each of these orientations.

The coordinates of reciprocal lattice points of ϕ_1 lying within 0.05 $Å^{-1}$ of the fluorite reciprocal lattice planes $\langle 110\rangle_f$, $\langle 112\rangle_f$, and $\langle 332\rangle_f$ were calculated for all 12 orientations of ϕ_1 with respect to the subcell. Some of the data, showing points that lie within 0.01 $Å^{-1}$ of the $\langle 332\rangle_f$ planes and at which diffracted intensity is allowed by the space group, are plotted in Fig. 3. When these patterns are superimposed, the patterns in Fig. 4a are obtained and it can be seen that the positions of most of the spots in the experimental data (Fig. 4d) are reproduced. This result indicates that the domain explanation of the data is substantially correct and that a fit to the experimental data should be obtained by taking the intensities of the reflections into account in addition to their positions.

4.2. *Calculation of Diffracted Intensity*

The intensities of the reflections whose positions are plotted in Fig. 4a (i.e., points lying within 0.01 $Å^{-1}$ of the plane) were calculated using atomic positions that have been proposed for ϕ_1 (*9*). This structure was derived from X ray powder intensity data, and while the positions and ordering of the hafnium and calcium ions are probably correct, the location of the oxygen vacancies is less certain. Also, because of limitations on the number of observations, the anions were assumed to occupy ideal fluorite positions.

In the first instance, the diffraction of electrons from individual small domains of ϕ_1 was assumed to be kinematic, and the Ewald sphere was regarded as a plane containing all the subcell reciprocal lattice points. Structure factors, calculated using scattering factors for electrons (*15*) were squared to give the required intensities. The distribution of intensity at each point was assumed to be spherical, with a Gaussian profile

$$I = I_0 \exp(-\pi D^2 z^2),$$

where D is the domain diameter; and z the distance from the point (Laue's approximation).

The data for domains 100 Å in diameter are plotted in Fig. 4b; the area of each spot is approximately proportional to the corresponding intensity. There is a reduction in the number of spots compared to the purely geometrical case (Fig. 4a) since many reflections are very weak, but the correspondence with Fig. 4d is poor.

4.3. *Double Diffraction*

It is inevitable that multiple scattering processes will occur in an electron diffraction experiment of this nature. Any diffracted beam within a crystal can act as a source beam for further scattering. In effect, a given kinematic diffraction pattern will have superimposed on it a number of similarly oriented kinematic patterns, each displaced so that the undeviated beam coincides with a diffraction spot, and each pattern is weighted according to the intensity of the source reflection. The intensity of any given spot therefore consists of several contributions, and differs from that expected on kinematic grounds.

In the present case, the calculated patterns shown in Fig. 4b were extended to the three similar quadrants around the origin using the symmetry operations relevant to the space group of ϕ_1 (a center of inversion and a diad or mirror line through the 220_f-type reflection). The effect of double diffraction within this region was taken into account by translating these extended patterns (without rotation) so that their origins coincided with each of the subcell reflections in turn, and summing the intensity contributions at each point. The subcell reflections were assumed to have the same intensity as the undeviated beam, and were given equal weight. The supercell reflections, because their intensities were very small by comparison with the subcell reflections, were not considered as sources of double diffraction.

The results for domains 100 Å in diameter, shown in Fig. 4c, are a reasonably good representation of the observed data in Fig. 4d. Variations of the domain diameter by

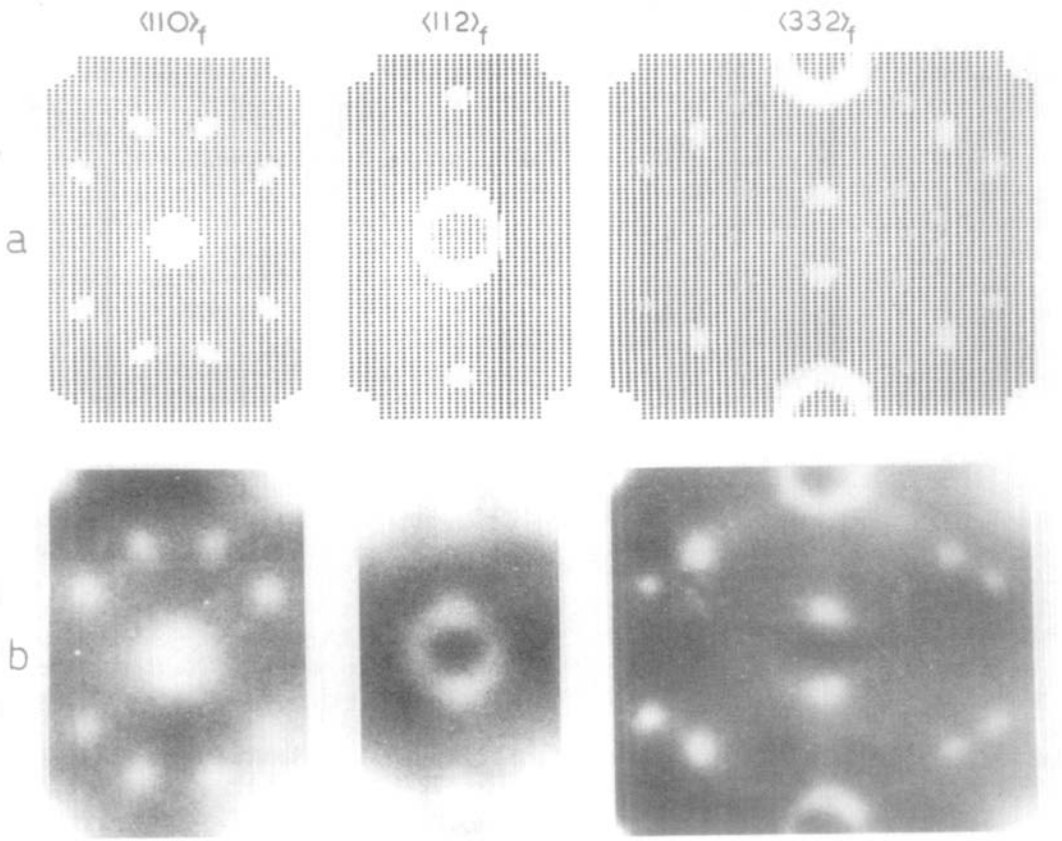

FIG. 5. Computed and experimental electron diffraction patterns from the high temperature cubic phase in the system CaO–HfO_2. (a) Patterns expected from a structure consisting of domains of ordered ϕ_1, 30 Å in diameter and 20 Å thick in the direction of the electron beam; the domains occur in 12 different orientations with respect to the fluorite-type matrix; subcell reflections lie at the corners of each pattern and at the center of the $\langle 110 \rangle_f$ pattern. (b) Experimental patterns, recorded from thin fragments of HfO_2–20 mole% CaO, prepared by arc-melting. The $\langle 110 \rangle_f$ and $\langle 112 \rangle_f$ patterns were recorded from samples as prepared; the $\langle 332 \rangle_f$ pattern was from a sample annealed in air at 1400°K for 60 hr.

50% resulted in a deterioration of the match between calculated and observed patterns: certain reflections that lay off the subcell planes tended to give inadequate contributions as the particle size was increased, whereas for smaller particles, undesirable contributions were collected from reflections centered further from the planes.

4.4. Application to the Microdomain Case

The procedures described above were applied to the case where the domains are reduced in size until the superlattice reflections become appreciably broadened. In this situation the plotting of points as in Fig. 4 is no longer appropriate; therefore the results are displayed in the form of computed halftone pictures (*16*). The diffraction patterns were simulated by rectangular arrays of appropriate dimensions, and the intensity at each point in the array was obtained by summing contributions from all reflections lying within 0.05 $Å^{-1}$ of the point, together with the contributions arising from double diffraction. The array was then output on a line printer, with the intensity at each point represented by a symbol of appropriate blackness. The domain size was varied until the calculated

diffraction patterns matched the experimental patterns reasonably well. The width of the diffuse maxima was quite sensitive to domain diameter, and a value of 30 Å gave a reasonable match with experimental data. Further improvement was obtained by reducing the thickness of the domains parallel to the electron beam to 20 Å. The effect of this was to enhance the contribution of off-plane reflections. The final computed patterns are shown in Fig. 5. together with experimental data recorded from arc-melted fragments of $Ca_{0.2}Hf_{0.8}O_{1.8}$.

Electron diffraction patterns from the disordered cubic phase in the zirconia–lime (Fig. 1a) and hafnia–lime (Fig. 5b) systems are very similar, suggesting that the same kind of microdomain model, based on the structure of ϕ_1, is applicable in both cases. This suggestion was investigated by computing the $\langle 112 \rangle_f$ pattern for a microdomain structure in which the hafnium ions in ϕ_1 were replaced by zirconium. The result was essentially the same as that shown in Fig. 5a, except that the intensity of the diffuse scattering was lower by a factor of about 3, as a consequence of the lower scattering power of zirconium relative to hafnium.

5. Discussion

Most of the features observed in electron diffraction patterns from lime-stabilized zirconia and hafnia can be explained satisfactorily in terms of a structure containing domains of the ordered phase ϕ_1. The agreement between observed and computed patterns is remarkably good in view of the number of approximations involved in the calculations. This agreement is to some extent superficial, because the averaging effect of double diffraction tends to suppress any discrepancies that might result from the approximate treatment. The relative importance of various possible sources of error is discussed below.

(*a*) *Domain orientations.* We have assumed that all possible orientations of the supercell of ϕ_1 with respect to the fluorite-type subcell are equally represented within the volume of material selected for electron diffraction. There is no reason to doubt this assumption when the domains are very small (e.g. Fig. 5), but it cannot be true as the domain size increases, since after long annealing single orientations of the ordered structure can be identified (Fig. 1c). An inspection of a number of patterns of the kind shown in Fig. 4d revealed differences in detail that could be attributed to the breakdown of this assumption when the domains have grown to 300 Å or more in size. For example, the spots labelled X in Fig. 4c ($\langle 332 \rangle_f$ pattern) do not appear in the experimental pattern in Fig. 4d, but they were found in other $\langle 332 \rangle_f$ patterns from similar samples.

(*b*) *Atomic positions in* ϕ_1. The intensities of the reflections from ϕ_1 were calculated using incomplete structural data (*9*); in particular the oxygen ions were assumed to occupy ideal fluorite positions. The inclusion of correct (but at present unknown) oxygen positions would alter the superlattice intensities slightly. Calculations were made for a ϕ_1 structure in which the oxygen ions were relaxed from their fluorite positions towards the vacant sites by distances similar to those observed in the related structures of ϕ (*8*) and ϕ_2 (*9*); the resulting patterns were only marginally different from those of Fig. 4. Individual kinematic intensities of superstructure spots varied by up to 50% from those calculated using unrelaxed anions, but these changes were smeared out by double diffraction.

(*c*) *Kinematic scattering.* The assumption that the scattering is kinematic implies a linear increase of intensity with thickness of crystal. In the case of electrons, the intensity of a particular diffracted beam returns to values close to zero periodically as the thickness increases, and the kinematic calculation is a reasonable approximation only for thicknesses less than perhaps 100 Å. As the domain size increases beyond this point, dynamical effects will become all-important. On the other hand, because the domains exist in 12 different orientations, it is likely that whatever their true shape may be, they present a range of thicknesses to the electron beam that will average the dynamical effects in some complicated way. The results suggest

that in this situation, the simple kinematic calculation is a reasonable approximation and that the neglect of dynamical effects has not introduced serious discrepancies.

(*d*) *Double diffraction.* The treatment of double diffraction assumes that only the strong subcell reflections are significant sources, and that each of these has equal weight. In addition, only a restricted region of the diffraction pattern (that represented by the experimental data in Fig. 1) was considered. These assumptions lead to patterns containing symmetry elements additional to those required by the space group. This added symmetry in the pattern of intensities is seen by comparing Figs. 4b and 4c. The same trend is obvious in the experimental data (Figs. 1a, 1b, 4d, and 5b) but there are differences in detail that are most probably due to the neglect of outer reflections.

(*e*) *Curvature of the Ewald Sphere.* In all calculations, the intensity at a plane in reciprocal space has been considered, whereas it is more correct to obtain the intensity at the surface of the Ewald sphere. Since the reflecting sphere lies wholly to one side of the plane, it might be expected that this would provide a means of enhancing the contribution from off-plane reflections. When the curvature of the Ewald sphere was taken into account, the contributions from some outer reflections were modified considerably, but after including double diffraction, the results were indistinguishable from those given in Figs. 4 and 5.

(*f*) *Domain size.* The scale of the mottled contrast in electron micrographs of thin fragments (e.g., Fig. 2) may be taken as an approximate indication of domain size, i.e., 50 Å for the disordered samples, increasing to 300 Å after short periods of annealing at 1500–1700°K. However, estimates obtained by matching the corresponding electron diffraction patterns with computed patterns were considerably smaller than this, i.e., 30 Å in diameter for disordered samples, increasing to 100 Å after annealing. In addition, the small domains were truncated to 20 Å in the beam direction to improve the match with experimental data. The effect of this truncation was to enhance the contribution from off-plane reflections. In the case of the larger domains, the diameter was selected on the basis of its effect on the contribution from off-plane reflections.

While both estimates of domain size are subject to considerable error, we believe that there are two major reasons for the discrepancies between them: (i) Misorientations of individual domains with respect to their neighbors; and (ii) real effects due to departures from spherical or near-spherical domain shape.

The calculation of positions of the supercell reciprocal lattice points was based on an accurately cubic subcell matrix, whereas in fact, small distortions of the order of 0.2% accompany the formation of ϕ_1. When the domains are small these distortions may be accommodated elastically, and probably give rise to the fine-scale mottled contrast in electron micrographs of disordered material (Fig. 2a). At this stage, it is unlikely that the distortions will have any significant effect on the positions of the reflections. However it might be expected that as the domains grow, the local mismatch at their boundaries would increase to an extent that would cause them to tilt with respect to one another. The enhancement of contrast in electron micrographs (Fig. 2b) that accompanies domain growth is consistent with this suggestion. When the domains are about 300 Å in size, tilts of about 1° would be sufficient to enhance the contribution from off-plane reflections by amounts comparable to those obtained by reducing the domain size to 100 Å. Thus, we believe that tilting of the domains becomes increasingly important as the domains grow, and that the domain size of about 300 Å, derived from the contrast in electron micrographs (Fig. 2b) is a better estimate than the 100 Å derived by matching experimental and computed diffraction patterns (Fig. 4).

When the domains are small, their shape will have an important influence on the appearance of the diffuse maxima in the diffraction patterns. It might be reasonable to expect that the ordered superstructure would develop along certain preferred directions, leading to the growth of domains that are platy rather than spherical in shape. If this

is the case, the intensity distribution in reciprocal space will be spiked in directions perpendicular to the faces of the plates. Because the plates occur in a variety of orientations, the spikes will lie at several different angles to the electron beam, but those that are close to parallel with the beam will be effective in enhancing the contribution of off-plane reflections to the diffraction pattern. Those that lie at greater angles to the beam, in general, will be less effective, but any contribution they do make will be displaced from the expected position in the pattern. These effects are difficult to compute, but evidence for both can be seen in the patterns in Fig. 5. Thus, it was found that a better match with experiment was obtained by truncating the domains from 30–20 Å in the beam direction. Secondly, there is a slight discrepancy in the positions of some of the diffuse spots in the experimental and computed $\langle 110 \rangle_f$ patterns that may well be due to contributions from spikes that lie at larger angles to the beam.

6. Conclusion

The major features in electron diffraction patterns from the high-temperature cubic phase in the systems $CaO–Zr(Hf)O_2$ are adequately accounted for in terms of a structure consisting of coherent micro-domains, coexisting in 12 different orientations within the cubic matrix. Within each domain, the structure is ordered and corresponds to that of ϕ_1, $CaHf_4O_9$.

Acknowledgments

We wish to thank Dr. H. G. Scott for many helpful discussions during the course of this work.

References

1. F. Hund, *Z. Physik. Chem.* **199**, 142 (1952).
2. T. Y. Tien and E. C. Subbarao, *J. Chem. Phys.* **39**, 4 (1963).
3. D. Michel, *Mater. Res. Bull.* **8**, 943 (1973).
4. C. Delamarre, *Rev. Int. Hautes Temper. et Refract.* **9**, 209 (1972).
5. C. Delamarre and M. Perez y Jorba, *C. R. Acad. Sci. Paris* **261**, 5128 (1965).
6. C. Delamarre and M. Perez y Jorba, *Rev. Hautes Temper. Refract.* **2**, 313 (1965).
7. J. G. Allpress, H. J. Rossell, and H. G. Scott, *Mater. Res. Bull.* **9**, 455 (1974).
8. H. J. Rossell and H. G. Scott, *J. Solid State Chem.*, **13**, 345 (1975).
9. J. G. Allpress, H. J. Rossell, and H. G. Scott, *J. Solid State Chem.*, to appear.
10. D. Michel, *Rev. Int. Hautes Temper. Refract.* **9**, 225 (1972).
11. R. E. Carter and W. L. Roth, *in* "Electromotive Force Measurements in High Temperature Systems" (C. B. Alcock, Ed.), Elsevier, New York (1968).
12. D. Steele and B. E. F. Fender, *J. Phys. C: Solid State Phys.* **7**, 1 (1974).
13. J. Billingham, P. S. Bell, and M. H. Lewis, *Acta Cryst.* **A28**, 602 (1972).
14. M. Sauvage and E. Parthé, *Acta Cryst.* **A28**, 607 (1972).
15. Lonsdale, K. (Ed.), "International Tables for X-ray Crystallography," Vol. III, Kynoch Press, Birmingham (1962).
16. A. K. Head, *Aust. J. Phys.* **20**, 557 (1967).